

Grazing-incidence Small-angle Scattering as a Tool for Thin Film Microstructure and Interface Analysis

Hiroshi Okuda, Shojiro Ochiai, M.Ohtaka*, Tetsu Ichitubo*, Ei-ichiro Matsubara*, Noritaka Usami**, Kazuo Nakajima**, Sono Sasaki*** and Osami Sakata***

International Innovation Center, Kyoto University, Sakyo-ku Kyoto 606-8501

Fax: 81-75-753-5193, e-mail: okuda@iic.kyoto-u.ac.jp

*Graduate School of Mater. Sci. Eng., Kyoto Univ. Sakyo-ku Kyoto 606-8501

**Institute of Materials Research, Tohoku University, Katahira, Sendai 980-8751

***JASRI, Kohto, Sayo, 679-5198

Several applications of grazing-incidence small-angle scattering (GISAXS) on the microstructural evolution at and near the surface as well as static evaluations of metallic and semiconducting nanodots are presented. The advantages of GISAXS over other methods, including transmission SAXS and microscopy are shown. By using GISAXS, static structure of even single layer of nanodots can be evaluated, including their interface abruptness.

Key words: GISAXS, semiconductor nanodots, Si-Ge, In-situ GISAXS, Fe-Pd-Cu alloys

1. INTRODUCTION

Grazing-incidence small-angle X-ray scattering (GISAXS) is one of the most growing fields in nanostructure analysis of thin films and near-surface microstructures using scattering techniques. From pioneering works by Levine et al., [1] that examined gold nanoparticles on Si substrates and Babboneau et al. [2] on co-sputtered Ag/C nanocomposites, GISAXS has been applied to evaluate nanostructures of self-organized heterostructures of inorganic, in particular, metal- and semiconductor- based nonequilibrium alloy systems. Although application of GISAXS is now blooming in soft-matter fields, in particular polymer thin films, hard materials are still interesting and important targets for this experimental method. For example, interface abruptness and the stability of heterointerface upon pseudomorphic overgrowth or annealing are known to be important in quantum well and superlattice structures [3-4]. Therefore, they should also play quite important role in the performance of quantum dot structures. Yet, there has been no clear result concerning the relationship between the interfacial interdiffusion and the performance of the self-assembled nanodots. Another important point in semiconducting nanodots is the strain field associated with the heterostructure. Although there are several well-defined experiments [5-6] that used wide-angle x-ray scattering (WAXS) around some fundamental Bragg points, these are still limited to quite large nano (or we should call it sub-micron) dots, where effect of strain is known to emerge clearly on the surface. In the present paper, a couple of GISAXS applications are introduced with some discussions on possible future extensions.

2. METHODS

GISAXS is a new field in small-angle scattering experiments. It is sensitive to surface and very thin films, which is a quite useful feature to examine advanced

nanomaterials which are often grown by strongly far-from-equilibrium conditions at the surface of well-defined substrates. From experimental viewpoint, GISAXS is a part of SAXS experiments in that it requires optics that give quite low parasitic scattering, and measurements are made without any receiving slits that cut undesirable scattering. Another aspect of GISAXS is that it is closely related to reflectivity measurements in that, the angle of incidence is usually very close to the angle of total reflection, and therefore, the sample treatment is very close to that of reflectivity /diffuse scattering measurements. Therefore, GISAXS measurements may be made either by introducing sample stage for reflectivity into a small-angle scattering beamline, or by introducing SAXS optics and detectors into a reflectivity beamline. In the following section, there two approaches on semiconducting nanodots will be shown. On the other hand, simultaneous SAXS and WAXS in grazing incidence is not simple, since the WAXS area of interest for the sample is not necessarily covered under grazing incidence conditions. This point will be discussed later.

3. EXPERIMENTAL

3.1 GISAXS and GISWAXS experiments at a SAXS beamline BL15A, Photon Factory

Since most of the requirements on optics for GISAXS are common to transmission SAXS, the most efficient way to realize GISAXS experiment is to use SAXS beamline in synchrotron facilities. Therefore, GISAXS measurements have been initiated in SAXS beamlines. Figure 1 shows a GISAXS trial at the beamline 15A of Photon Factory, Tsukuba, first examined in 1999. After the storage ring and the beamline mirror were modified for high brilliance in 1997, the beamline has become suitable also for GISAXS experiments. As shown in the figure, the incident beam was fixed at 0.15 nm and focused on the detector position. The position of

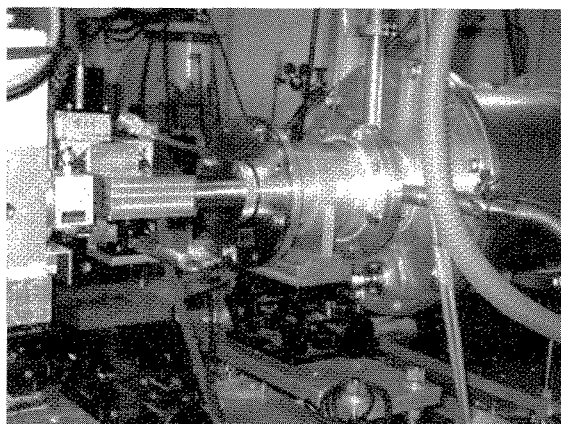


Fig. 1 GISAXS apparatus implemented at beamline 15A of Photon Factory, Tsukuba. The sample stage was evacuated to prevent air scattering.

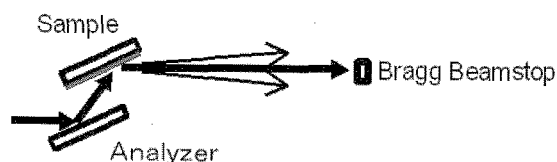
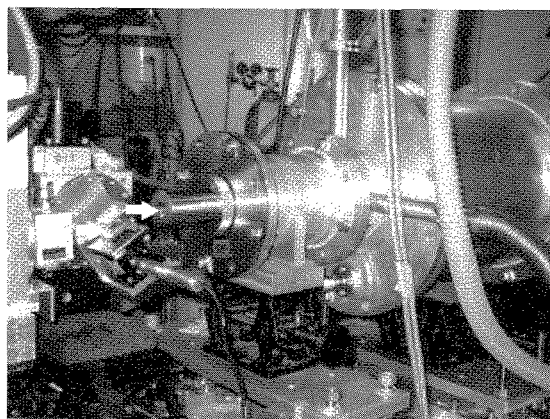


Fig. 2 Two-dimensional in-situ WAXS measurements at the SAXS beamline 15A. 9-inch II-CCD was attached at the back end for in-situ measurements.

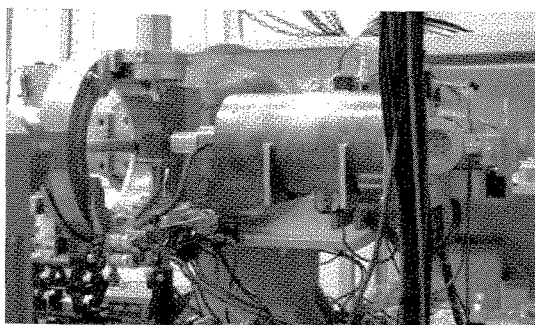


Fig. 3 A SAXS measurement system mounted on a diffractometer at BL-13XU of SPring8. A SAXS sample holder and beam paths were mounted on a Kohzu multiaxis diffractometer at the beamline.

specular reflection was monitored by a translucent beam attenuator.[7,8] By using the system, the structures of buried Ge nanodots having Si cap layer grown by molecular beam epitaxy (MBE) have been examined.[8]

For WAXS measurements at a SAXS beamline, we have proposed two approaches. One is a simple extension of scattering vector, that is quite similar to the conventional transmission SWAXS measurements[9]. The other one may make sense only for epitaxial and almost perfect samples. The sample position of the latter approach is shown in Fig. 2. It consists of a pair of substrates in double crystal (+/-) geometry. The front one is a bare substrate used to orient the incident beam, and the rear one is the sample having the same substrates.

The merit of using this geometry is that the diffracted beam, i.e., doubly diffracted incident beam runs parallel to the incident beam. Then the two-dimensional detectors such as image-intensified CCD (II-CCD) or imaging plate (IP) detectors need not to be moved vertically up to the Bragg position. Since the incident beam is linearly polarized in horizontal direction for bending-magnet beamlines, it is also not desirable to measure the high-angle diffraction/ scattering intensity in horizontal direction. Although the acceptance for the first (front) crystal is not large enough for the focusing SAXS beamline, this method is now under development for simple WAXS (diffuse scattering) mapping.

3.2 GISAXS at beamline 13XU, SPring8.

The other GISAXS approach described in the previous section is to introduce SAXS apparatus into a reflectivity beamline. Figure 3 is a photograph of GISAXS experiments that is mounted on a multiaxis goniometer[8]. Although this approach has a drawback that heavy two-dimensional detectors are hardly mounted, the angle of incidence and the sample position can be far better defined by the slit systems mounted on the goniometer. In the present measurements, the effect of heat treatment of Ge nanodots grown by GS-MBE was examined by GISAX recorded on imaging plates.

3.3 In-situ Experiments of GISAXS at 40B2, SPring8

An important aspect of GISAXS experiment is to inquire into the self-organization process at surface or in very thin layers. For this purpose, time-resolved measurements is indispensable. Since in-plane and out-of-plane structure is different in thin films, it is essential to use two-dimensional detectors in time-resolved mode. From a technical viewpoint, however, this gives rise to a difficult technical problem for time-resolved measurements. At present, two-dimensional detectors used for time-resolved SAXS experiments are either II-CCD or CCD with optically coupled phosphor. Two-dimensional multiwire position sensitive detectors (PSD) developed for conventional source easily saturate, or were even burn down on GISAXS measurements at 2nd / 3rd generation sources. However, II-CCD has limited dynamic range, and phosphored CCD does not have enough sensitivity for very weak scattering. Therefore, we need to choose either high sensitivity and speed without large dynamic range,

or larger dynamic range with low sensitivity.

In the present measurements, we carried out time-resolved GISAXS measurements on the formation process of iron based alloy nanodots from uniform thin films with II-CCD, which requires only the Guinier regions, and dynamic range is not essential. Temporal evolution of GISAXS pattern was recorded in-situ during heating the sample up to 723 K in a sample chamber evacuated by turbo molecular pump.

4. RESULTS AND DISCUSSIONS

4.1 Static analysis of Ge nanodots capped with Si

As well known as capillary effects, small nanodots are expected to be more unstable than larger ones, and may disappear by interdiffusion during growth of a cap layer. Several researchers [5-6][10] have reported that the Ge nanodots grown by MBE or other techniques such as liquid phase epitaxy (LPE) may already lose its initial (designed) composition by intermixing during the growth, and eventually the composition changes with the height of the nanodots. This is a serious problem for designing nanodots as devices, since the controlling composition of the nanodots is then not the matter of suppressing interfacial diffusion, but the matter of changing growth kinetics itself. However, since these reports used rather high growth temperatures, it is worthwhile checking if capped nanodots grown at relatively low temperature maintain its shape and interface structures. A GISAXS pattern of Ge nanodots grown by MBE and capped with about 40 nm of Si layer is shown in Fig. 4. The modulus of the scattering vector, q , is defined by ;

$$q = 4\pi \sin \theta / \lambda \quad (1)$$

with λ the wavelength of the incident X-ray.

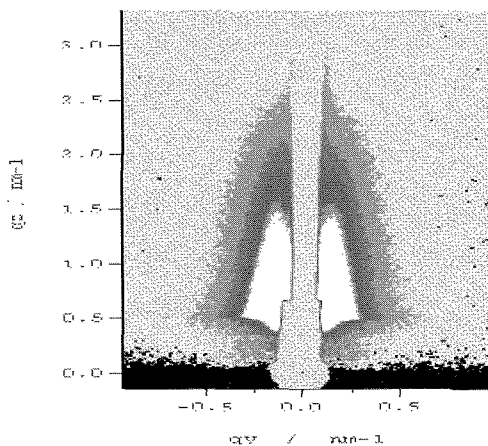


Fig. 4. GISAXS pattern for Si-capped Ge nanodots grown by MBE. 110 incidence and the angle of incidence of 0.5 degree. Well-defined bell-shaped scattering pattern with nanodot-nanodot correlation was observed. q_y in the figure corresponds to in-plane scattering vector, and q_z to the out-of-plane scattering vector.

As discussed in the previous papers [7],[11], the GISAXS patterns showed intensity elongated in the

direction normal to the substrate surface, suggesting that the shape of the Ge nanodots is flat in the growth direction. The gyration radius corresponding to Fig. 4 is 9.3 nm in q_y direction and 3 nm in q_z direction. This result suggests that the analysis may be made by kinematical framework, since it means that the nanodots are small enough so that the SAXS intensity appears at the scattering vector far enough from the Yoneda line. This case, the analysis is quite simplified, since the Fourier transform of the GISAXS pattern represents the shape and the size of the nanodots in the region. Conventional SAXS analysis for transmission SAS is applicable to the results. To confirm this point, reflectivity and the penetration depth of the incident X-ray for the photon energy used in the present measurement was calculated and shown in Fig. 5. The reflectivity for the present condition is of the order of magnitude of 10^{-2} , with the penetration depth of about one micrometer. The figure is calculated for a flat Si substrate, and therefore the actual perturbation that gives the correction term (DWBA correction) should be even smaller, suggesting that the scattering intensity at larger q_z can be analyzed by BA approximation.

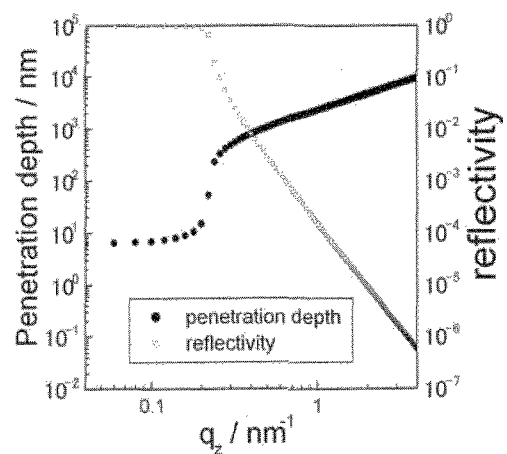


Fig. 5. Calculated reflectivity and penetration depth for an ideal Si substrate. It helps to evaluate the magnitude of correction expected in the DWBA analysis of the SAXS pattern.

From the above discussion, we may discuss power law behavior to examine whether the Ge nanodots encapsulated by Si layer have almost abrupt interfaces. For transmission SAXS, the power law behavior of SAXS intensity at large q region, so-called Porod's law, is often used as a measure to examine interface abruptness. The power law region at higher q may exhibit q^{-4} behavior for smooth and abrupt interface[12], whereas the slope changes depending on the nature of the interface, such as fractal structure or diffuse interface[12,13]. Figure 6 shows a vertical and a horizontal cross-sectional intensity profiles obtained for the Ge nanodots grown by low-temperature GSMBE.

The size of the nanodots estimated from Guinier approximation was 8.8 nm in q_y and 2.3 nm in q_z directions. From Fig. 6, the power law for the interface of the Ge nanodots grown by low-temperature GSMBE

is very close to -4 , meaning that the interface between Ge nanodots and the cap layer is rather abrupt. This is quite different from the preceding results on the large Si-Ge alloy nanodots reported by Schmidtbauer et al.[5,6] From practical viewpoint, large nanodots with submicrons of diameter is interesting for precise evaluation, since the scattering volume is large enough so that accurate measurements may be easier. However, the nanodots are of great interest when the size of the dots are of the order of the diameter of, e.g., excitons. Therefore, the present results suggesting that very small nanodots still maintain well-defined interface if the encapsulation is made at low temperatures. Since the power law shows a slight deviation from the -4 power law, the origin may be attributed to the growth of interfacial interdiffusion layer. More detailed analysis is now in progress.[14]

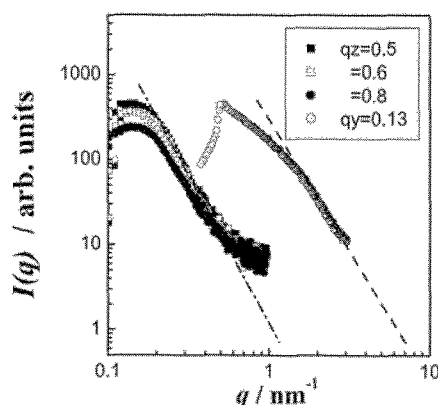


Fig. 6. GISAXS profiles along q_y / q_z directions as a function of q .

From the viewpoint of strain and composition distributions in the nanodot microstructures, however, the WAXS measurements described in the section 3.1 has still difficulties in measuring small nanodots as shown above, since the diffuse scattering is still very weak and technically it is difficult to separate the strain scattering and the form factor for such small nanodots from the thermal diffuse scattering (TDS) in the present equipments. Further developments of the low-temperature diffuse scattering measurement system should be required for the quantitative measurements for these small nanodots.

4.2 In-situ experiments on the nanodots formation in Fe-Pd-Cu ternary alloys

Fe-Pt and Fe-Pd based alloys are attracting attention as a new generation of hard magnetic material for recording. There has been several attempts to prepare perpendicularly magnetized nanostructures separated in a couple of nanometers each other, to realize ultra-high recording density.[15-17] To realize uniform nanostructures having well controlled vertical magnetization performance, it is essential to design the microstructure of the hard magnetic materials such that they are under complete order in the direction perpendicular to the substrate (e.g., $L1_0$ superlattice structure having c axis normal to the substrate) with in-plane direction artificially processed by, for example,

lithographic methods, or with in-plane direction having self-organized island structures. The latter case may be considered conceptually an analogue of Co-Cr based alloy systems, where spontaneously formed Cr segregation layer served as a separation between columnar Co grains. Fe-Pt based alloys with $L1_0$ ordered structure is one of the candidates that have attracted attention for the recording material with a nanodot microstructures[15,16]. To control the transformation temperatures and kinetics, several attempts on alloying effects have also been made. Among this, addition of Cu is reported to be effective to lower the ordering temperature[17]. From a viewpoint of phase transformation, the stability and ordering kinetics of nanodots and its relationship to the morphological transition from layered structure into separated nanodots is one of the interesting points.

The sample compositions of sputtered alloy films have been evaluated from Rutherford Backscattering Spectroscopy (RBS) measurements using He ions with 2 MeV of incident energy. The average composition determined by total yield of the ions at each energy was $Fe_{0.26}Pd_{0.29}Cu_{0.45}$. The Cu concentration was found to be larger than expected. Therefore, the samples used in the present experiments were not in the single phase region in the equilibrium state. The samples prepared by sputtering on Si substrates were mounted on an in-situ GISAXS stage evacuated with a rotary pump and then heated up to the annealing temperatures at the heating rate of 20 K/min.

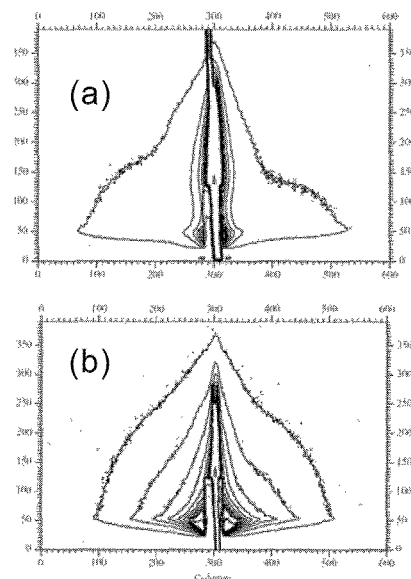


Fig. 7 GISAXS patterns for an Fe-Pd-Cu ternary sample heated at 0.33 K/s up to 723 K and then isothermally annealed. (a) at 590 K, (b) when the sample reached 723 K.

In-situ GISAXS measurements were made at BL-40B2 of SPring8, a small-angle scattering beamline, and BL-15A of Photon Factory. Time-resolved GISAXS patterns were measured by a 6-inch image-intensified CCD detector. The measurements started when the sample stage was heated up to 473 K, and then

measurements were made every 90 to 120 s up to 9 ks. Figure 7 shows a temporal evolution of GISAXS patterns during heating. These intensity maps have a strong streak in common, elongated along q_z direction at $q_y=0$. This component corresponds to the scattering from surface roughness, suggesting that the surface is not smooth even in the initial film state. At a rather low temperature of 590 K as shown in Fig. 7(a), diffuse scattering at the both wing around the roughness scattering is already observed as shown by a pair of circles in the figure.

These intensities correspond to the SAXS from the islands formed by annealing treatments. As easily noticed, one characteristic feature about the scattering profile is that the interparticle interference is hardly observed. This is quite different from most of GISAXS patterns obtained for nanodots densely distributed on substrates[18-20]. For example, Fe-Pt thin films annealed under external strong magnetic field[16], with well-separated nanodot structures observed by scanning electron microscopy (SEM), show well-defined interparticle interference peaks. Figure 8 shows a SEM image of the sample after the in-situ GISAXS experiment of annealing at 723 K for 7.3 ks. The micrograph shows an interconnected granular structures rather than circular islands separated each other in space. This microstructure agreed with the GISAXS profiles shown in Fig. 7, which does not show a typical interparticle interference in the in-plane (q_y) direction. One of the possible explanations is that the oxygen partial pressure is not low enough, because of the conductance of the sample chamber. Then the phase separation may be different due to formation of oxides which alters the surface energy that drives the morphological transition during annealing. At this moment this explanation remains a hypothesis since we do not have phase diagram and physical properties of the Fe-Pd-Cu-O system. However, recent results with better vacuum conditions tend to give well-separated nanodots, supporting the present discussion.

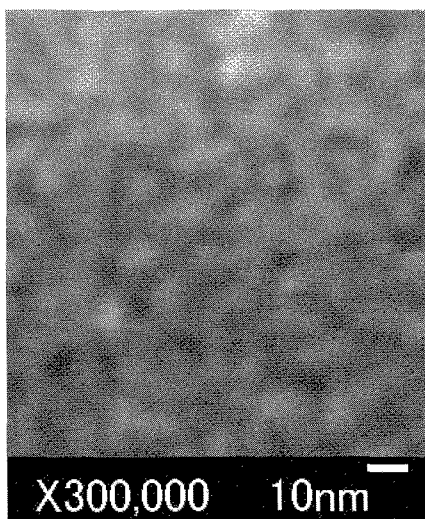


Fig. 8 SEM micrograph of a FePdCu sample after in-situ GISAXS measurement at 723 K for 7.3 ks.

As shown in Fig. 7, GI-SAXS intensity increased with time during annealing. In particular, it is noted that the scattering intensity from nanodots can be observed even during heating up the sample. The change of the average size of nanodots evaluated by gyration radius in z direction is shown in Fig. 9 along with the temperature of the sample measured by a thermocouple embedded in the copper plate just between the sample and a ceramic heater. It is clearly seen that the gyration radius increases at the early stage of heating process, even at a low temperature of 473 K, and the slowing down of the growth is clearly seen after the temperature reached the annealing temperature. This result suggests that the initial stage of island formation is fast, and begins even at the temperatures as low as 473 K or lower, where normally no appreciable diffusion should be observed. The present results imply that the morphological transition from a thin flat film into nanodots is mainly controlled by the instability of flat film microstructures, and normal Ostwald ripening is sluggish.

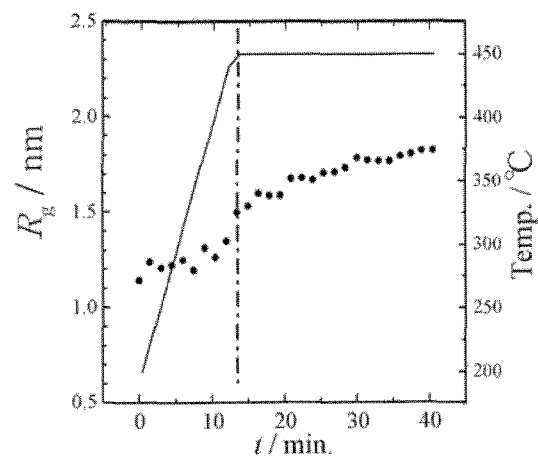


Fig. 9 Temporal evolution of gyration radius, R_g , in z direction perpendicular to the substrate with aging time. The solid line gives the temperature of the sample during in-situ measurements.

5. SUMMARY

Applications of GISAXS / GISWAXS to semiconducting nanodots and metallic nanodots have been discussed with some examples from our group at the SR beamlines currently available for GISAXS measurements. For semiconducting materials, structure of self-assembled nanodots with a size of about several to several tens of nanometers can be evaluated even if the dots are capped with a cap layer, if the thickness of the layer is reasonably small. This limitation on the thickness of cap layer may restrict availability of GISAXS to some device-oriented layer structures. Still, it is worthwhile examining what happens at the early stage of embedding nanostructures. Concerning GISAXS on metal nanodots, application of these techniques to the hard magnetic dots are just in the beginning of the research, where the finite scale effects on ordering kinetics, temperatures, and microstructural stability is yet to be examined. In the field of metallic nanodots, in particular, many researches have been made

in Europe and in the US, at the beamlines equipped with in-situ ultra-high vacuum growth chamber. Domestic research is in this sense far behind the edge. From this viewpoint, combined (multi-probe) and wide-q-range / anomalous studies, such as GISWAXS or GI-Anomalous SAXS (GI-ASAXS) under external field for example, may contribute to give a new insight in this field.

References

- [1] J.R.Levine, Y.W. Chung, J. Cohen, P. Georgeopoulos, *J. Appl. Cryst.*, 22, 528-534 (1989).
- [2] D.Babboneau, A. Naudon, A.Thiaudiere and S. Lequien, *J. Appl. Cryst.*, 32, 226-233(1999).
- [3] Y. Takeda, *Trans. Mater. Res. Soc. Japan*, 28,11-14 (2003).
- [4] M.Tabuchi, K.Fujibayashi, N. Yamada, K.Hagiwara, A.Kobayashi, Y.Takeda, H.Kamei, *J. Cryst. Growth* 186, 48-57(1998).
- [5] I. Kegel et al., *Appl. Phys. Letters*. 74 2978-2980 (1999).
- [6] M.Schmidtbauer et al. *Cryst. Res. Technol.* 37,3-6 (2002).
- [7] H. Okuda, S. Ochiai, K. Ito and Y. Amemiya, *Appl. Phys. Letters*. 81,2358-2360(2002).
- [8] H.Okuda, M.Ohtaka, S.Ochiai, *J. Jpn. Soc. Synchrotron Rad. Res.* 19,419-427(2006). (japanese)
- [9] H.Okuda, , K. Osamra, Y.Amemiya, M.Osawa, and K. Ito, *J. Appl. Cryst.* 30,585-590(1997).
- [10] M.Schmidtbauer, *X-ray Diffuse Scattering from Self-Organized mesoscopic semiconductor structures*, Springer,Berlin, 2004.
- [11] T.Ogawa, , H.Niwa, T. Tsukimoto, H. Okuda and S. Ochiai, *Mater. Sci. Forum*, 475-479, 1097-1100, (2005)
- [12] O.Porod,: in '*Small-angle X-ray scattering*', ed. by O. Glatter and O. Porod , Academic Press, N.Y.,1983.
- [13] T. Viscek, '*Fractal Growth*' World Scientific, Singapore, 1992.
- [14] M. Ohtaka, T.Ogawa, H. Okuda, S.Ochiai, SAS2006 Abstract, p130 (2006).
- [15] S. Momose, H.Kodama, T.Uzumaki and A.Tanaka, *Jpn. J. Appl. Phys.* 44, 1147-1149(2005).
- [16] T.Ichitsubo, M. Kojima, N.Kawashima and M.Hirao, *Jpn. J. Appl. Phys.* Pt.1 42,2858-2859(2003).
- [17] T.Maeda T.Kai, T.Nagase and J.Akiyama, *Appl. Phys. Letters*. 80, 2147-2149(2002).

(Received December 9, 2006; Accepted February 23, 2007)